CHAPTER IV
RESULTS AND DISCUSSION

4.1 Base Case Experiment

The base case experiment was a 300mL solution of 170mM monosilicic acid ($Si(OH)_4$) and 4M hydrochloric acid (HCl) at 5.0°C and 500rpm. Samples were withdrawn at different times, filtered through a 0.2μm PP filter, and characterized using ICP/MS. Figure 4.1 shows the concentration of Si in filtered samples as a function of time. At ~1,964 minutes, the measured Si concentration decreased drastically, representing the end of the plateau region. At approximately 1,964 minutes, particles greater that 0.2μm had formed in the solution and were unable to permeate through the 0.2μm filters. Consequently, Si could not be seen with the ICP and the concentration of Si in withdrawn samples decreased drastically. The time to reach 0.2μm was also consistent with DLS measurement (see Figure 4.2).

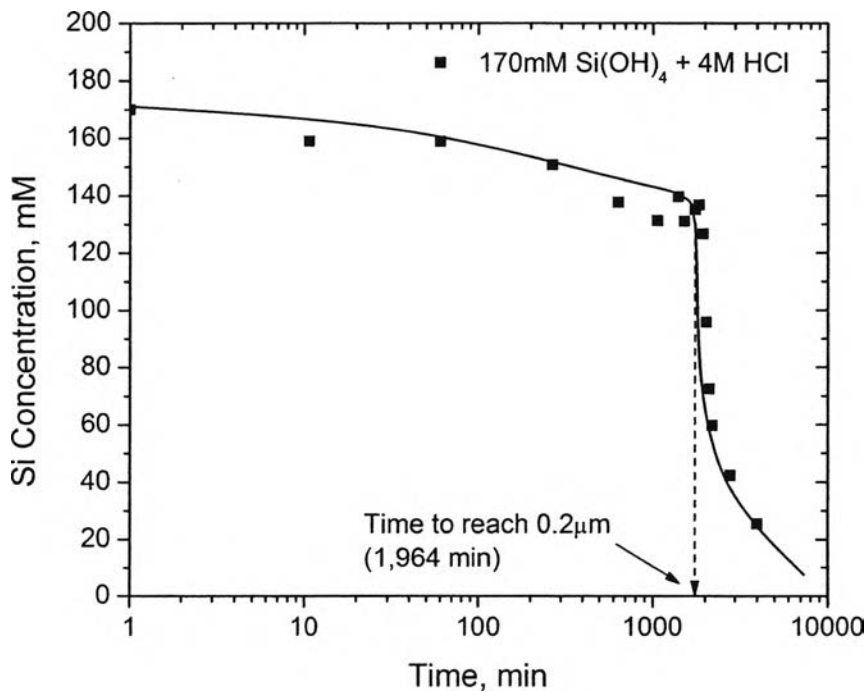

Figure 4.1 Concentration – time trajectory in 170mM monosilicic acid + 4M HCl solution (base case solution) measured by ICP/MS.

Silica particle sizes were also measured at different times using DLS and are shown in Figure 4.2. The mean silica particle size determined from the intensity as a function of particle diameter distribution was found to grow exponentially with time according to the relationship

$$D(t) = D_o \exp(k_G t) \tag{4.1}$$

where $D(t)$ = particle diameter with respect to time (nm),

D_o = initial particle size (nm),

and k_G = particle growth rate constant ($\frac{1}{\text{min}}$).

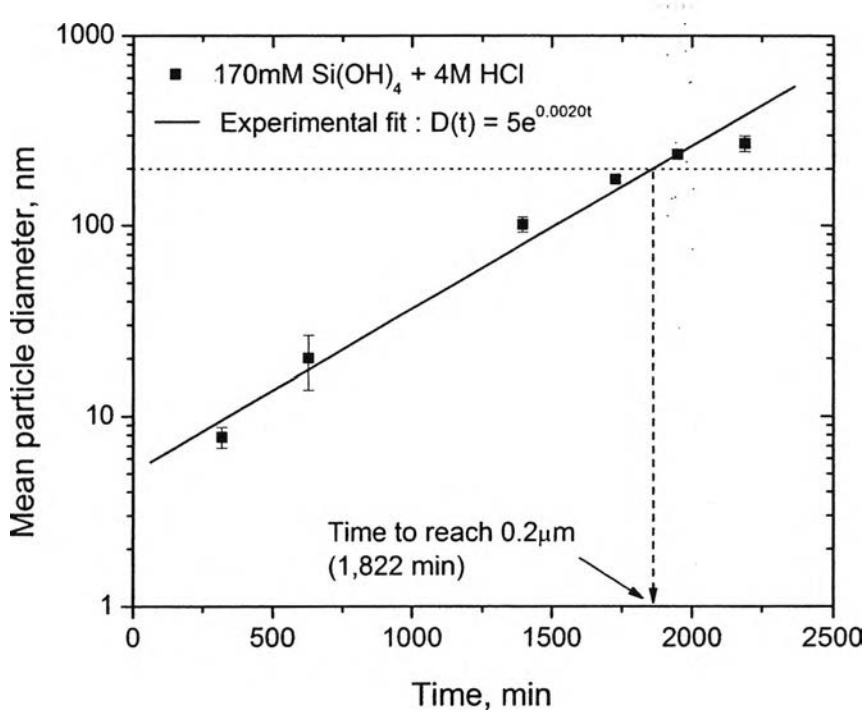

Figure 4.2 Mean silica particle diameter versus time for base case solution measured using DLS.

4.2 Salt Experiments: Precipitation Investigated Using ICP/MS and DLS Techniques

4.2.1 Chloride Salt Trials

A number of experiments were carried out where different chloride salts were added to the base case solution (170mM $Si(OH)_4$ + 4M HCl). NaCl, CsCl, $MgCl_2$, $CaCl_2$, and $AlCl_3$ were used to investigate their influence on particle growth and aggregation phenomena of silica suspensions. Figure 4.3 shows the Si concentrations withdrawn from the reactor as a function of time. The times to reach 0.2μm (the size at which is unable to permeate through PP filters) are in the order of

pure HCl (base case) > CsCl > NaCl > $MgCl_2$ > $CaCl_2$ > $AlCl_3$.

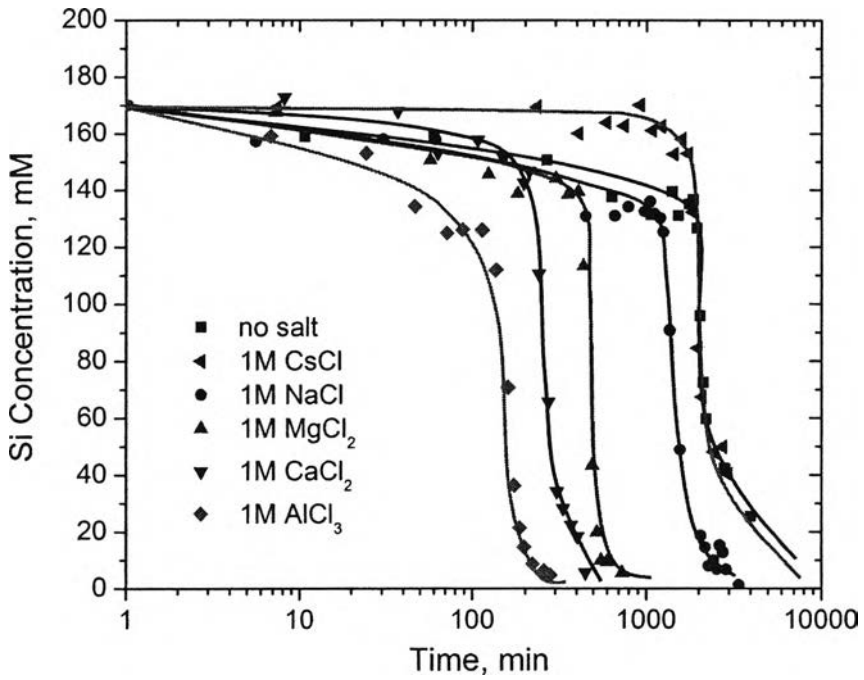

Figure 4.3 Si concentration profiles as a function of time obtained from different chloride salt solutions measured by ICP/MS.

DLS data show that the exponentially increasing growth model of silica particles used for the base case (Equation 4.1) is also valid for the chloride salts

trials. Among different chloride salts, the trivalent inorganic salt $AlCl_3$ at 1M is more effective at promoting particle growth than the divalent and monovalent salts at the same concentration, which follows the same order of salts obtained by ICP/MS.

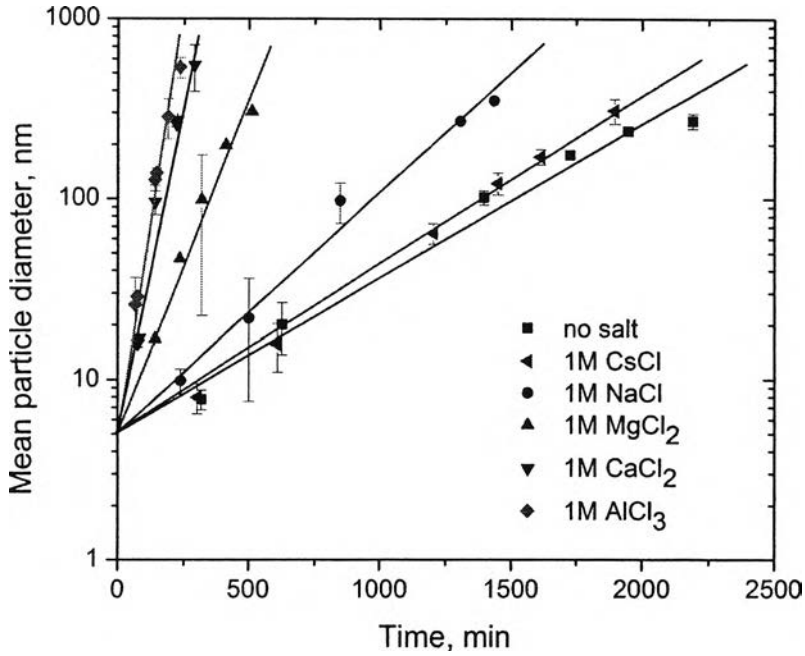

Figure 4.4 Growth in particle diameter size with time for chloride salts.

Table 4.1 Times required to reach 0.2μm analyzed using ICP/MS and DLS for different chloride salts.

Solution[§]	Time to reach 0.2μm observed from ICP/MS (min)	Time to reach 0.2μm measured from DLS (min)
4M HCl	1,964 ± 51	1,822 ± 26
4M HCl + 1M CsCl	1,695 ± 51	1,715 ± 5
4M HCl + 1M NaCl	1,125 ± 64	1,210 ± 5
4M HCl + 1M $MgCl_2$	447 ± 40	434 ± 2
4M HCl + 1M $CaCl_2$	210 ± 3	211 ± 2
4M HCl + 1M $AlCl_3$	133 ± 7	172 ± 2

[§] $[Si(OH)_4]_0 = 170mM$

4.2.2 Sodium Salt Trials

The influence of anions on silica precipitation was also investigated. In this part, four different sodium salts (NaCl, $NaNO_3$, NaBr, and NaI) were used to study the effect of different anions on silica particle growth and aggregation process. The times to reach 0.2μm are in the order of

$$\text{pure HCl (base case)} > NaNO_3 \sim NaCl > NaBr > NaI,$$

which corresponds to the ranking obtained from DLS results. The ICP/MS and DLS results are given in Figure 4.5 and 4.6, respectively.

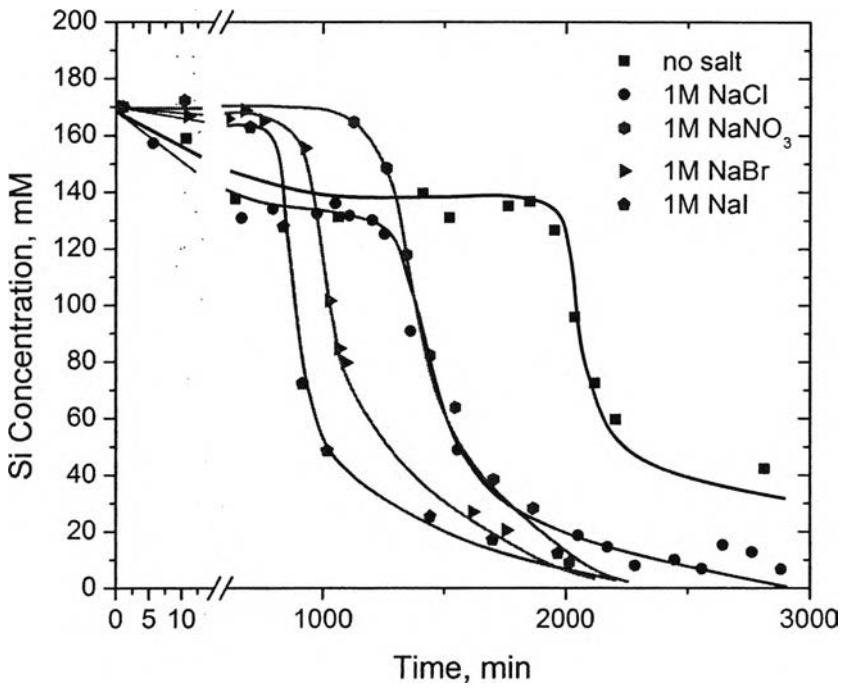

Figure 4.5 Si concentrations – time trajectory obtained from different sodium salt solutions measured by ICP/MS.

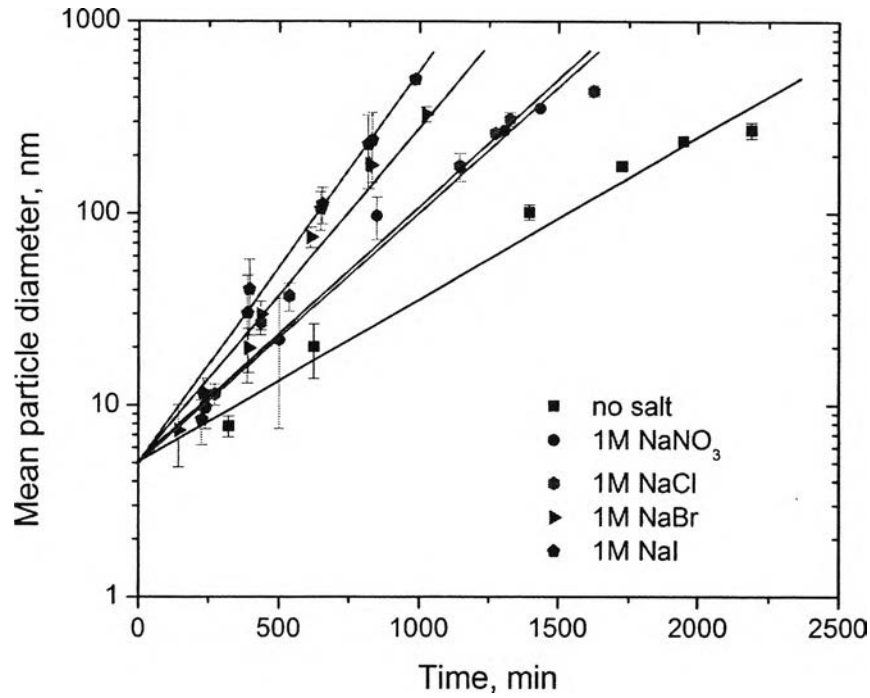

Figure 4.6 Growth in particle diameter size with time for sodium salts.

Table 4.2 Times required to reach 0.2μm analyzed using ICP/MS and DLS for different sodium salts.

Solution[£]	Time to reach 0.2μm observed from ICP/MS (min)	Time to reach 0.2μm measured from DLS (min)
4M HCl	1,964 ± 51	1,822 ± 26
4M HCl + 1M $NaNO_3$	1,230 ± 44	1,274 ± 63
4M HCl + 1M NaCl	1,125 ± 64	1,210 ± 5
4M HCl + 1M NaBr	918 ± 30	900 ± 29
4M HCl + 1M NaI	808 ± 33	780 ± 4

[£] $[Si(OH)_4]_0$ = 170mM

4.3 Analysis of Monosilicic Acid Disappearance Kinetics

The kinetics of the disappearance of monosilicic acid was investigated using the Molybdenum-blue method (ASTM D859-05) where UV-Vis spectroscopy was used to measure concentrations of monosilicic acid in solution. First, the numerical method was used to determine the reaction order of disappearance kinetics. In order to figure out this unknown, the simple concentration rate law was postulated;

$$\frac{d[Si(OH)_4]}{dt} = -k_D[Si(OH)_4]^m \tag{4.2}$$

where k_D and m are disappearance rate constant and reaction order, respectively.

Reaction order (m) trials were primarily investigated using UV-Vis results obtained from the base case experiment. UV-Vis data were statistically fitted with the reaction order m = 2, 3, and 4 to determine the best reaction order. The closed-form fitting equation for $Si(OH)_4$ was obtained by direct integration of equation (4.2) with m = 2, 3, and 4, yielding the relationships shown in Table 4.3. The determination of reaction order was carried out using numerical fitting and residual sum of square (RSS) statistical analysis.

Table 4.3 Analysis of reaction orders.

Reaction order (m)	Fitting equation	RSS value
2	$[Si(OH)_4] = \left(k_D t + \frac{1}{[Si(OH)_4]_o} \right)^{-1}$	1.404
3	$[Si(OH)_4] = \left(2k_D t + \frac{1}{[Si(OH)_4]_o^2} \right)^{-1/2}$	0.043
4	$[Si(OH)_4] = \left(3k_D t + \frac{1}{[Si(OH)_4]_o^3} \right)^{-1/3}$	0.243

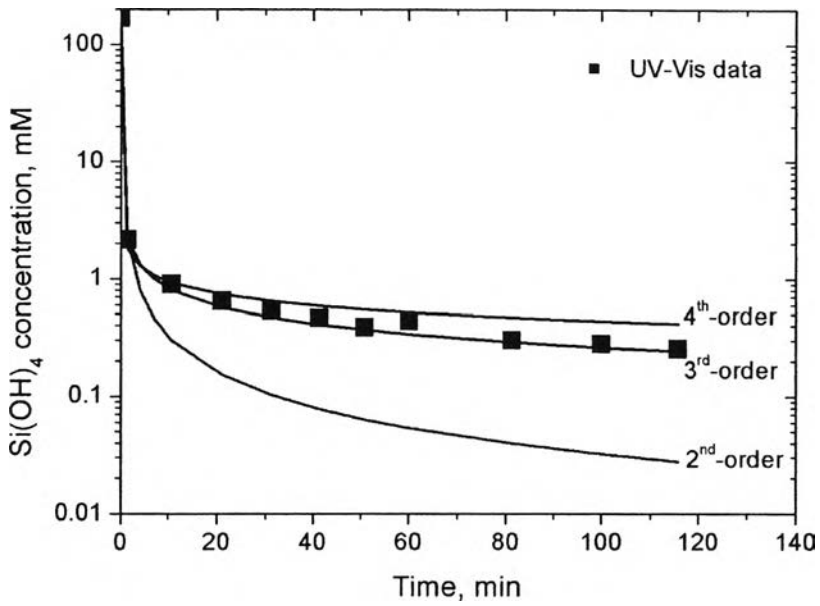

Figure 4.7 Reaction order trials on the base case experiment.

Using the residual sum of square (RSS) analysis, UV-Vis data showed that third-order reaction provides the best fit to our experimental data with the RSS value of 0.043, which means that third order is the best reaction order. This is, the kinetic of monosilicic disappearance obeys third-order rate law dependence. The rate equation of monosilicic acid disappearance could be written as

$$\frac{d[Si(OH)_4]}{dt} = -k_D[Si(OH)_4]^3 \tag{4.3}$$

where k_D denotes the disappearance rate constant ($\frac{1}{mM^2 \cdot min}$). Direct integration of equation (4.3) yields the following relationship;

$$\frac{1}{2}\left(\frac{1}{[Si(OH)_4]^2} - \frac{1}{[Si(OH)_4]_o^2}\right) = k_D t \tag{4.4}$$

UV-Vis results show that the third-order disappearance kinetics is also valid for the salt solutions. The plot of the rate function, $\frac{1}{2}\left(\frac{1}{[Si(OH)_4]^2} - \frac{1}{[Si(OH)_4]_o^2}\right)$, versus time for different salt systems are given in Figure 4.8 and 4.9. The disappearance rate constant k_D is obtained from the slope of the linear relationship between the rate function and time. The data show that the rate constants increase when salt was added to the acid solution. The different salts accelerate the kinetics of monosilicic acid disappearance in the following order;

$CaCl_2 \sim AlCl_3 > MgCl_2 > NaCl > CsCl$ for different chloride salts, and

$NaI > NaCl > NaBr > NaNO_3$ for different sodium salts.

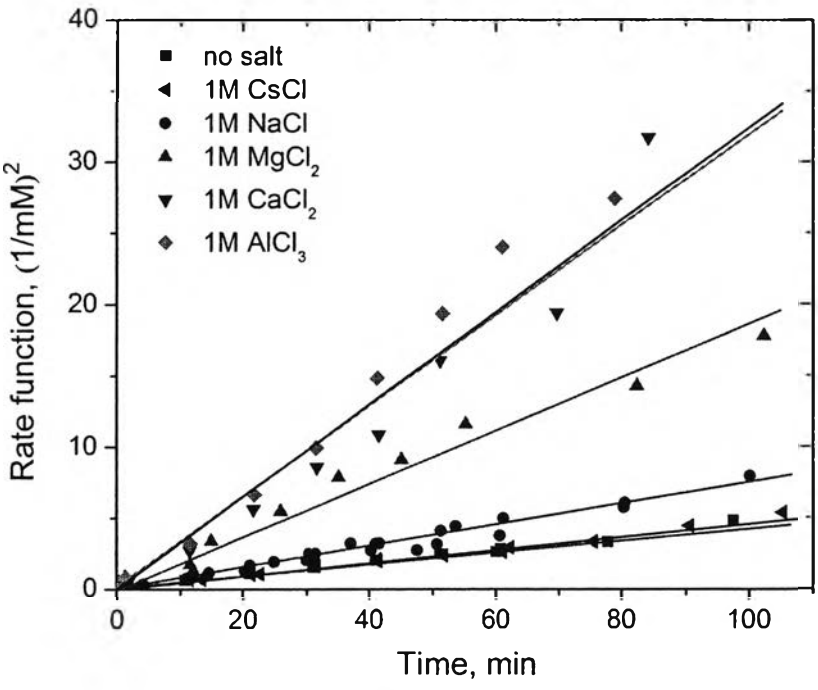

Figure 4.8 $\frac{1}{2}\left(\frac{1}{[Si(OH)_4]^2} - \frac{1}{[Si(OH)_4]_o^2}\right)$ versus time for chloride salts trials.

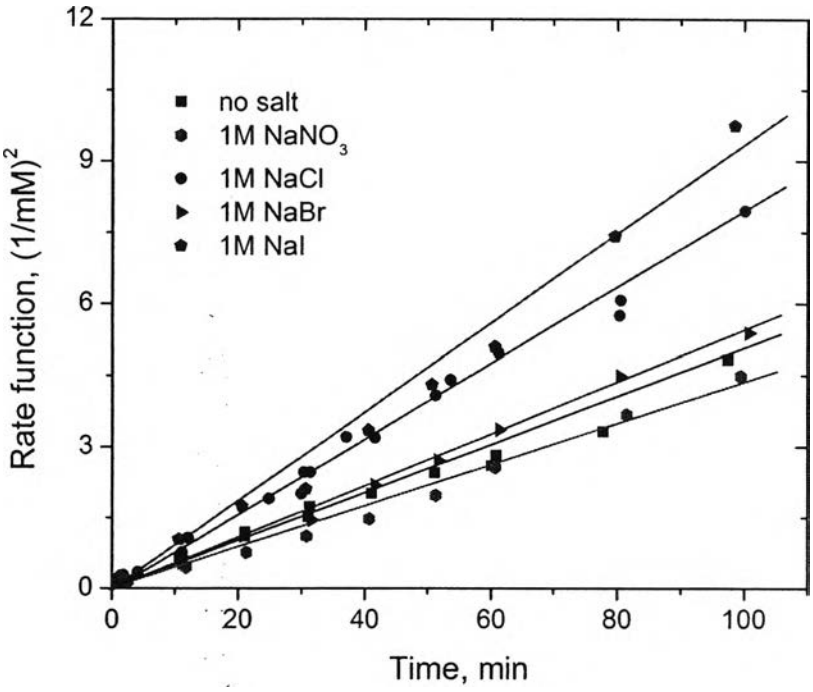

Figure 4.9 $\frac{1}{2}\left(\frac{1}{[Si(OH)_4]^2} - \frac{1}{[Si(OH)_4]_o^2}\right)$ versus time for sodium salts trials.

It has been noticed that total silica concentration, as measured by ICP/MS, is apparently found to be much higher that molybdate reactive silica concentration. The molybdate reactive silica test will expose monomers, possibly dimers, of silicic acid in the solution whereas ICP/MS will detect the total amount of silica species permeating through PP filters (less than 200μm).

4.4 Particle Growth Predictions Using Geometric Population Balance Equations

From UV-Vis and DLS experiments, they establish that monosilicic acid monomers disappeared from solution very rapidly and the exponential growth was observed throughout the course of experiment as shown in Figure 4.10. The next step would be to investigate mechanisms of silica particle growth. From Figure 4.10 points out that the disappearance of silicic acid monomers happened quickly while silica particles grew exponentially with the starting diameter of 5nm at t=0. One

could hypothesize that possible mechanisms of silica particle growth would be the aggregation of silica primary particles; not condensation polymerization.

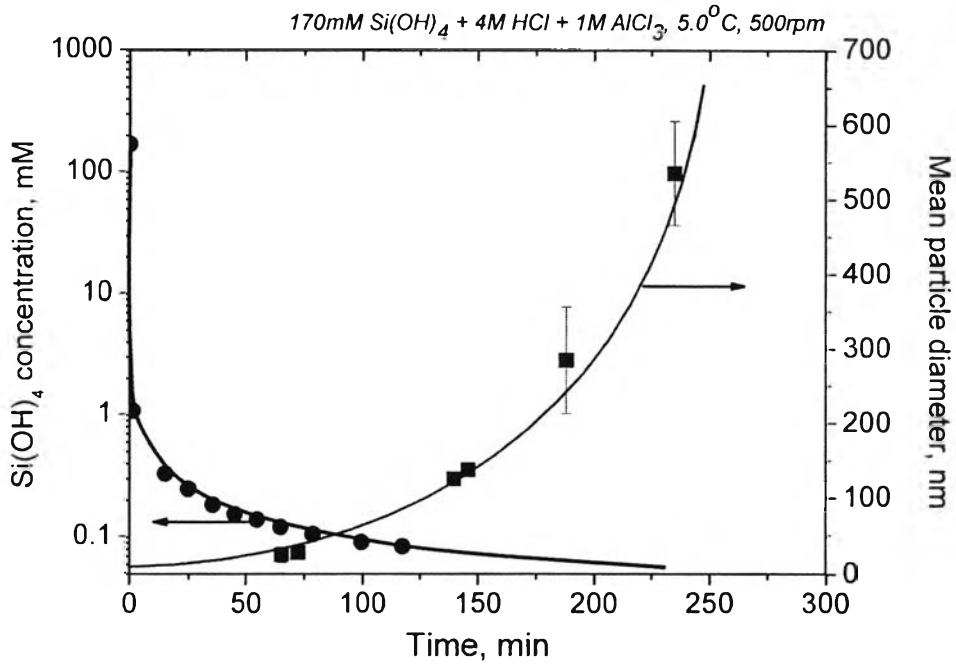

Figure 4.10 Particle growth and remaining monosilicic acid concentration vs. time.

The modified Smoluchowski equation for colloidal aggregation under the framework of geometric population balance equations (GPE) was used to study the mechanism of silica particle growth and predict the particle growth patterns as a function of time. The modified Smoluchowski equation is expressed as given

$$\frac{dn_i}{dt} = \frac{K_{i-1,i-1}}{R} n_{i-1}^2 + n_{i-1} \sum_{j=1}^{i-2} \frac{R^{j-1}}{R^{i-1} - R^{i-2}} K_{i-1,j} n_j - n_i \sum_{j=1}^{i-1} \frac{R^{j-1}}{R^i - R^{i-1}} K_{i,j} n_j - n_i \sum_{j=1}^{N-1} K_{i,j} n_j \qquad (2.7)$$

The aggregation process was modeled with a geometric spacing (R) of 2. That is, the i-th aggregate of the discretized system contains 2^{i-1} number of primary particles; for example, the forth aggregate has 2^3 (or 8) primary particles. A conceptual scheme of this model is illustrated in Figure 4.11.

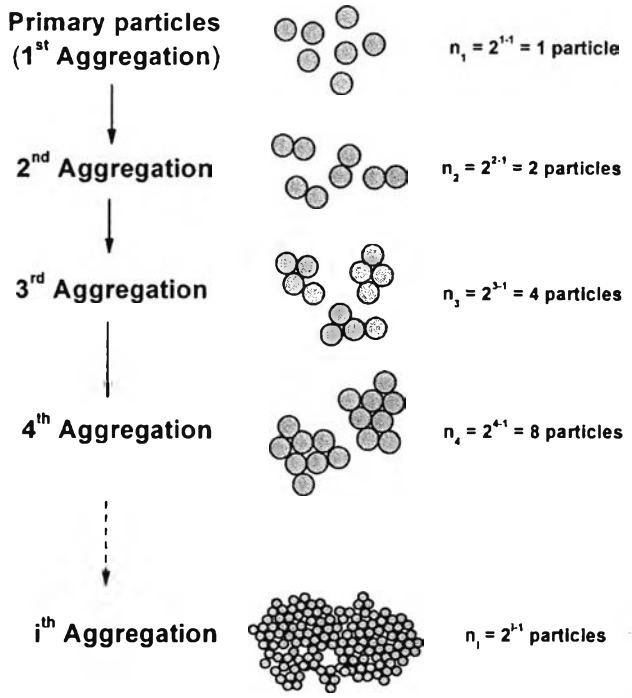

Figure 4.11 Conceptual scheme of aggregation model for geometric spacing R = 2.

The particle sizes used for modeling ranged from 5nm to 0.1mm and the discretized population balance equation (Equation 2.6) was divided into 30 geometric sections for aggregates containing 1, 2, 4, …, $2^{(30-1)}$ primary particles. The resulting 30 non-linear ordinary differential equations were solved simultaneously in MATLAB® `ode23` function.

The important parameters that needed to be identified for modeling were collision kernel and the size of primary unit. In this study, an estimated primary silica particle size obtained from DLS of ~5nm and the collision kernel for reaction-limited aggregation were used in the model, assuming that (1) silica particles form primary particles of 5nm instantly and (2) aggregation is reaction-limited. The expression of reaction-limited collision kernel is given in Equation 4.5 (see derivation in *Appendix A*);

$$K_{ij} = \frac{1.0404 R_g T}{\eta D_p^2} (D_i + D_j)^2 \beta \qquad (4.5)$$

where R_g = universal gas constant (8.314 $\frac{J}{mol \cdot K}$),

T = absolute temperature (K),

η = viscosity of the medium (cP),

D_p = diameter of primary particle (nm),

β = collision efficiency,

and $D_{i(j)}$= particle diameter of i-th (j-th) aggregate (nm).

The simulated particle size profiles based on the reaction-limited aggregation (RLA) kernel are shown in Figure 4.12. One observes that the development of silica aggregate size matches with the mean particle size data gained from DLS for all salts studied and that the RLA model well describes the evolution of silica particle size, which confirm that the assumption that the primary particles are formed at t=0 is acceptable and that the aggregation mechanism is reaction-limited.

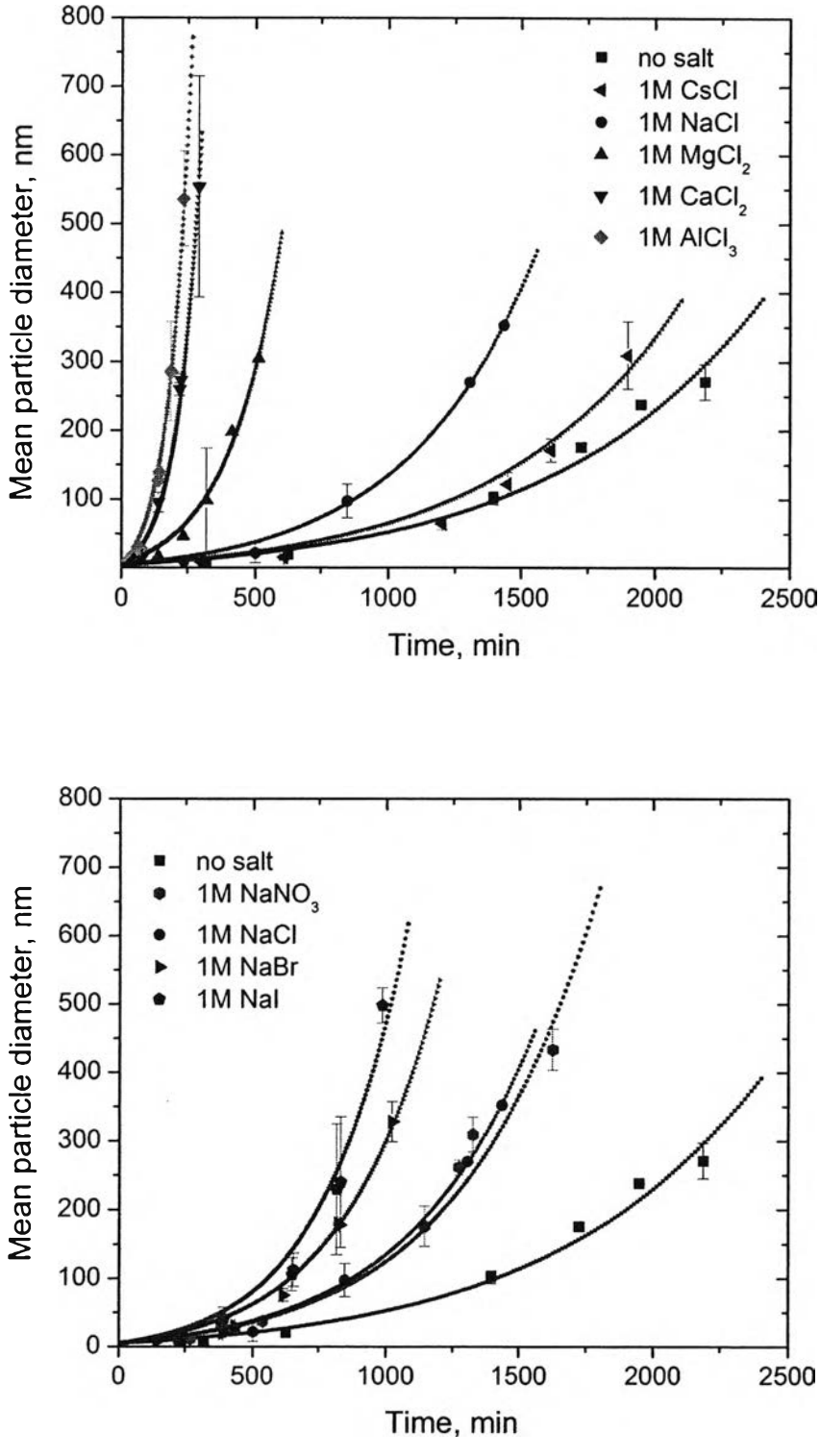

Figure 4.12 Comparison of the evolution of silica particles between experimentation (dots) and simulation (dashes) using RLA model; (top) Chloride salts and (bottom) Sodium salts.

The evolution of particle size as a function of time simulated in conjunction with the geometric population balance equations provided the systematic approach for estimating the size of the silica aggregate. The RLA model is able to determine the time needed to reach 0.2μm, which could be compared with the results obtained from ICP/MS and DLS.

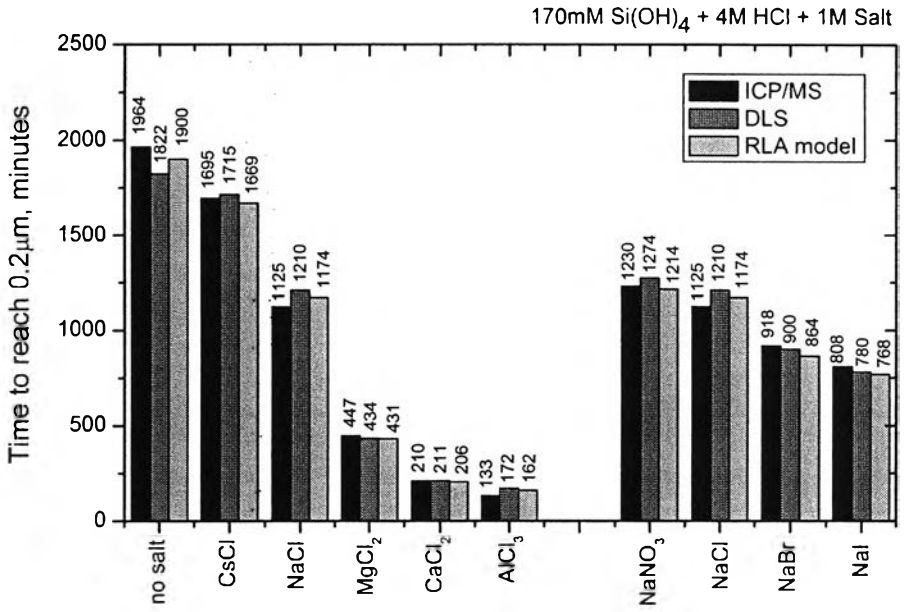

Figure 4.13 Times to reach 0.2μm obtained from different salts and different techniques.

Figure 4.13 presents the comparison of times to reach 0.2μm observed from 3 different approaches, and shows the good agreement between ICP/MS, DLS data and simulated data from RLA model. One concludes that the presence of 1molar of salt hastens the particle growth in order of

$AlCl_3 > CaCl_2 > MgCl_2 > NaCl > CsCl$ for different chloride salts, and

$NaI > NaBr > NaCl \sim NaNO_3$ for different sodium salts.

Table 4.4 Comparison of particle growth rate constants (k_G), disappearance rate constants (k_D), and collision efficiency (β) obtained from salt experiments.

Solution	Ionic strength (M)	k_G $(\frac{1}{min})$	k_D $(\frac{\times 10^4}{M^2 \cdot min})$	β
170mM $Si(OH)_4$ + 4M HCl (basecase)	4	0.0020 ± 0.0000	6.13 ± 1.63	1.787×10^{-11}
Chloride Salts Trials				
170mM $Si(OH)_4$ + 4M HCl + 1M CsCl	5	0.0024 ± 0.0000	4.52 ± 0.58	1.979×10^{-11}
170mM $Si(OH)_4$ + 4M HCl + 1M NaCl	5	0.0031 ± 0.0001	8.26 ± 0.81	3.053×10^{-11}
170mM $Si(OH)_4$ + 4M HCl + 1M $MgCl_2$	7	0.0090 ± 0.0006	23.18 ± 8.09	1.002×10^{-10}
170mM $Si(OH)_4$ + 4M HCl + 1M $CaCl_2$	7	0.0175 ± 0.0001	46.36 ± 14.29	1.962×10^{-10}
170mM $Si(OH)_4$ + 4M HCl + 1M $AlCl_3$	10	0.0216 ± 0.0001	46.21 ± 14.45	2.233×10^{-10}
Sodium Salts Trials				
170mM $Si(OH)_4$ + 4M HCl + 1M $NaNO_3$	5	0.0030 ± 0.0001	5.71 ± 1.62	2.889×10^{-11}
170mM $Si(OH)_4$ + 4M HCl + 1M NaCl	5	0.0031 ± 0.0001	8.26 ± 0.81	3.053×10^{-11}
170mM $Si(OH)_4$ + 4M HCl + 1M NaBr	5	0.0042 ± 0.0002	5.64 ± 0.11	4.509×10^{-11}
170mM $Si(OH)_4$ + 4M HCl + 1M NaI	5	0.0047 ± 0.0001	9.05 ± 0.86	4.663×10^{-11}

4.5 Ionic Strength Studies on Silica Aggregation

Fleming (1986) studied the dependence of ionic strength on polymerization rate constant of silica system in near-neutral circumstances using the Debye-Hückel law. It was shown that the rate constants depend on the activity coefficients of the monosilicic acids, which in turn are a function of the ionic strength. Fleming also proposed an empirical relationship between ionic strength and the rate constants. The relationship is shown below;

$$\ln k_p = A x_I + B \tag{4.6}$$

where k_p = polymerization rate constant,

x_I = ionic strength function ($x_I = \frac{\sqrt{I}}{1+\sqrt{I}}$),

$I = \frac{1}{2}\sum_{i=1}^{n} Z_i^2 C_{i,\infty}$ = ionic strength ($\frac{mol}{dm^3}$),

Z_i = charge number of ion *i*,

$C_{i,\infty}$ = molar concentration of ion *i* in bulk solution ($\frac{mol}{dm^3}$),

and A, B = empirical constants.

The following relationship was applied to the silica system in this *low pH* system. To investigate the effect of ionic strength on silica aggregation, a set of $AlCl_3$ experiments was conducted. For the sake of providing the wide study range of ionic strength, the solutions of 170mM $Si(OH)_4$ + 4M HCl + xM $AlCl_3$, where x = 0.083, 0.333, 0.552, and 1.000, were prepared and experiments were performed at the same analogous conditions. Figure 4.14 shows the dependence of ionic strength on particle growth rate and collision efficiency. This plot was constructed by normalizing all values to the base case (k_{G° = 0.0020 min^{-1}, $\beta^\circ = 1.79\times10^{-11}$, and x_{I° = 0.667). The experiments establish that particle growth rate constants (k_G, Eqn

4.1) and collision efficiency (β, Eqn 4.5) increase exponentially with respect to the ionic strength function.

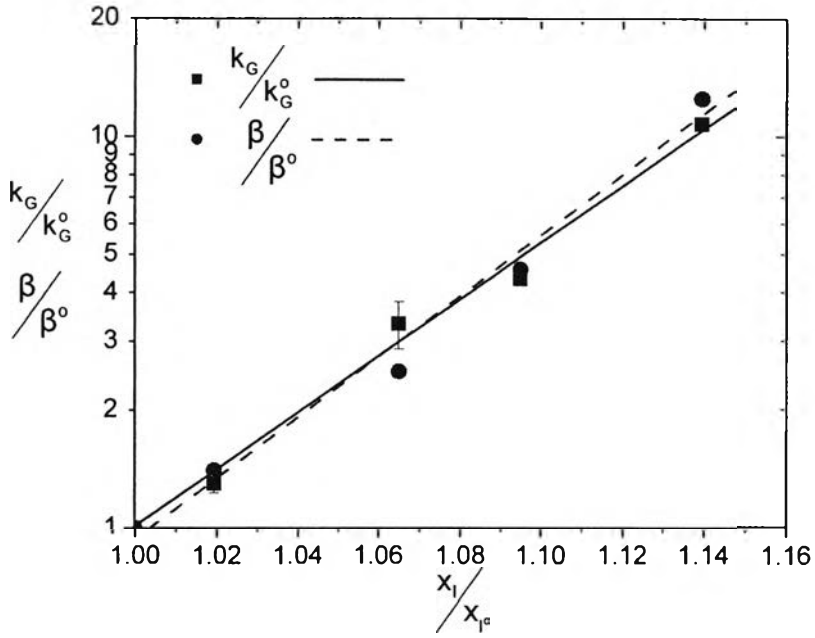

Figure 4.14 Dependence of the normalized particle growth rate constant ($\frac{k_G}{k_{G^\circ}}$) and collision efficiency ($\frac{\beta}{\beta^\circ}$) on the function of normalized ionic strength (x_I/x_{I°), obtained from $AlCl_3$ experiments.

Moreover, the normalized k_G and β values of different salt systems were also compared and are shown in Figure 4.15 and 4.16, respectively. One observes that the aggregation of silica particles are promoted as the ionic strength of the solution increases. At the same molar concentration of salts, it was found that a trivalent salt system (i.e. $AlCl_3$), which causes the highest ionic strength, exhibits the greatest impact on silica aggregation/precipitation as compared to the monovalent salt systems (i.e. NaCl, CsCl, $NaNO_3$) which have the smallest effect. In addition, the influence of ionic strength on the disappearance rate constant (Figure 4.17 where $k_{D^\circ} = 6.13\times10^4$ molar^{-2}.min^{-1}) was determined and the exponential trends of those three parameters were also observed.

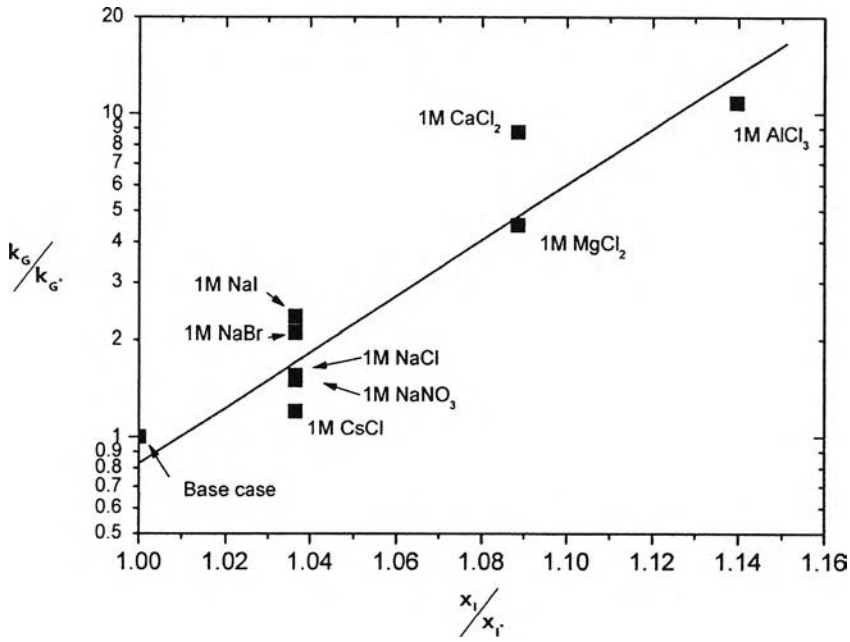

Figure 4.15 Dependence of the natural logarithm of particle growth rate constant on the ionic strength function.

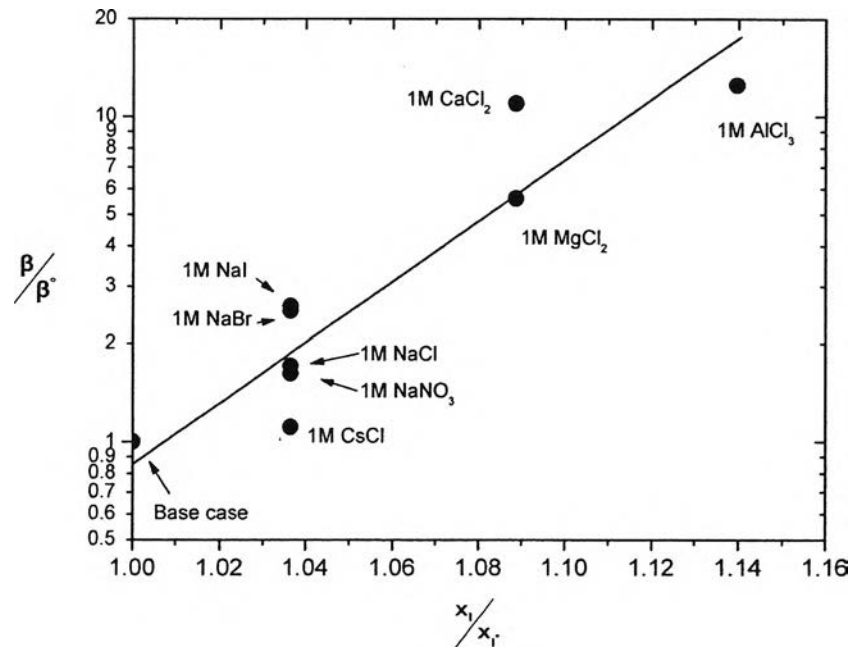

Figure 4.16 Dependence of the natural logarithm of collision efficiency on the ionic strength function.

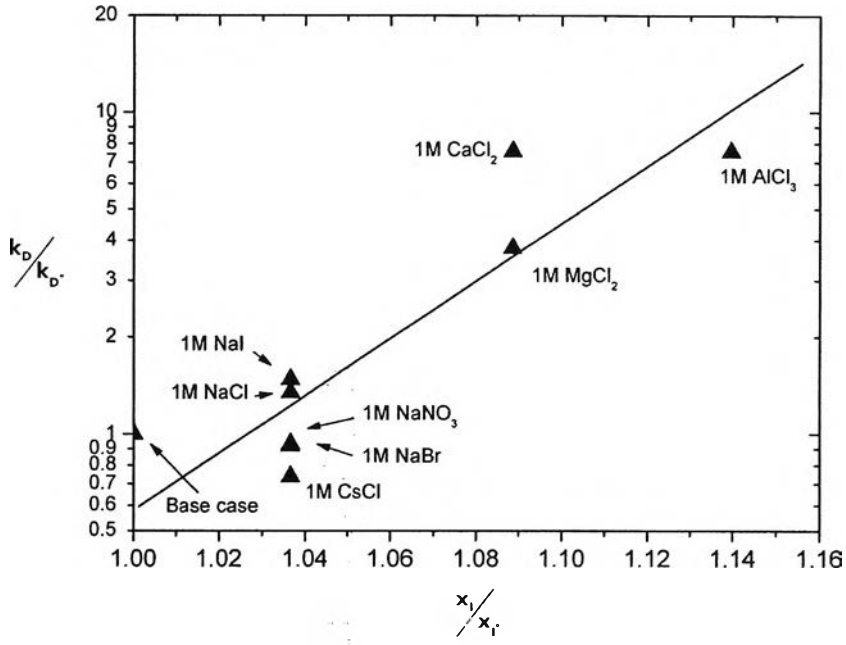

Figure 4.17 Dependence of the natural logarithm of disappearance rate constant on the ionic strength function.

4.6 Hypotheses for Salt Experiments

The interaction between charged colloidal particles in a liquid medium has been explained in terms of classical Derjaguin-Landau-Verwey-Overbeek (DLVO) forces, i.e. attractive van der Waals force and repulsive electrical double layer force. The sum of DLVO forces can determine the stability of colloidal particles in solution. The colloidal stability decreases when the repulsive force is larger than the attractive one. From a practical point of view, the stability of suspended particles decreases as the ionic strength of the medium increases because the increase in ionic strength reduces the electrical double layer thickness and thus weakens the repulsive force (Ogonowski *et al.*, 2008). The weakened repulsive force enables two colloidal particles to attract to each other more easily, resulting in the coagulation of particles.

However, fast aggregation in the case of high ionic strength silica system is not only the result of the weakened repulsive force. In our high ionic strength systems, the double layer thickness was calculated to be around 0.9Å which is

extremely small, compared to the size of hydrogen atom of ~1Å (see *Appendix B*). Consequently, classical DLVO forces cannot completely describe the interaction of silica particles due to the occurrence of an additional short-range repulsive force.

The origin of this non-DLVO force has been investigated by a number of researchers. Several workers believe that the silica particle itself is strongly bound to water molecules. This additional force may arise from surrounding water molecules, preventing two suspended particles to approach one another, referred to as "hydration forces". Other researchers hypothesize that this repulsive force may arise from the existence of "silica hairs", which are silanol groups (Si-OH) and silicic acid groups ($Si\text{-}O^-$) protruding from the surface of silica particles. There protruding groups may contribute to the steric force to prevent two particles coming into contact. However, the satisfied explanation of this non-DLVO force is still inconclusive.

Based on those two competing theories, one could hypothesize the role of salt on fast silica aggregation/precipitation as following;

1. *Hydration force theory*: The water bound to the silica particle surface acts as a barrier to flocculation, and the salt (ion) interrupts the ordering of the bound water and acts as a bridging agent to connect silica particles together via oxygen-coordinated bonding, causing fast flocculation.

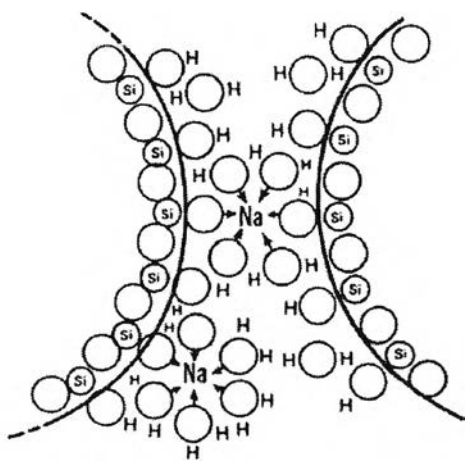

Figure 4.18 Possible bonding between silica particles through coordination with salt (ion) (Iler, 1979).

The ability of salt ions to link/bridge two silica particles together could be explained by the hydration number, which gives the conventional number of water molecules surrounding on the first layer round the ion. In this system, bound water molecules come from water molecules bonded coordinately with silica particles or silica surfaces. Instead of the conventional hydration number, it is more preferential to explain in term of an 'apparent hydration number', which is the number accounting for the average effect of all ion-water interactions and governing contributions from water molecules outside the first layer. Figure 4.19 shows the correlation between the apparent hydration number and particle growth rate constant. It was found that values of k_G tend to increases as hydration number increases. By rationalization, we may conclude that higher hydration number could lead to the higher degree of bridging, which in turn leads to the faster aggregation.

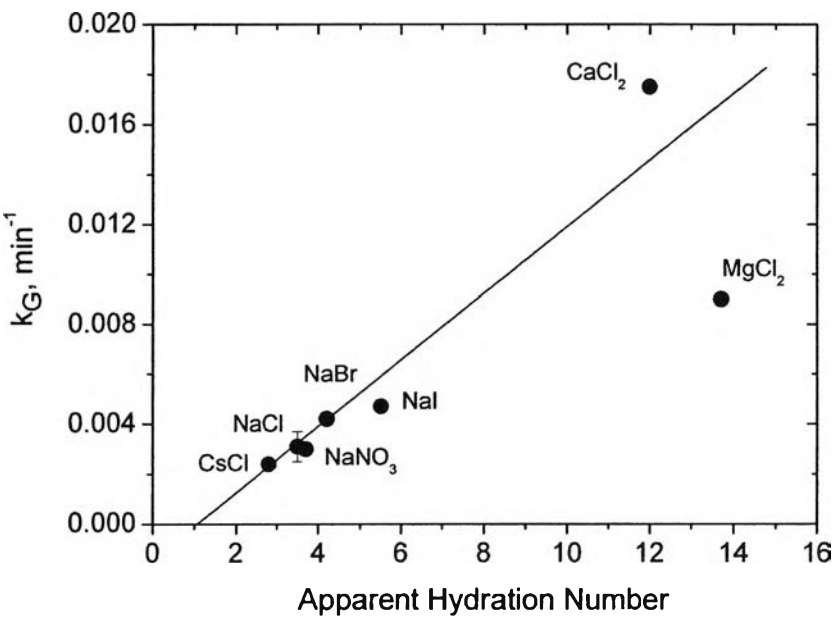

Figure 4.19 Particle growth constants (k_G) from one-molar-salt experiments at 5.0°C compared with some apparent hydration numbers for chloride and sodium salts. Apparent hydration numbers were compiled from data given by Stokes and Robinson (1984), and Max and Chapados (2000).

2. *Silica hairs theory*: Silicon groups protruding from silica surfaces give rise to a repulsive steric force. The presence of salt causes these silica hairs to lay flat on the silica particle surface offering less steric resistance and rapid aggregation.

To describe the laying-down phenomenon completely presents no easy task because the mechanism is not yet explored and well-defined. The author believes that the possible mechanism could be similarly explained by the bridging theory but the bridging in this case favorably takes place between a hydroxyl group of the protruding silica hair and a neighboring silica surface. By applying the bridging theory, the higher hydration number would result in the higher amount of laying-down silica hairs which leads to the substantial weakening of steric repulsion and to the fast flocculation/aggregation finally.

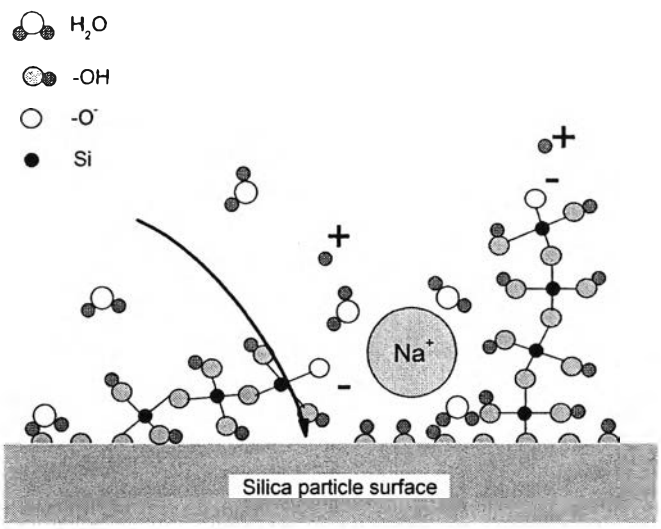

Figure 4.20 Silica hairs laid flat on the silica surface result in the less steric repulsion.